Available online at www.sciencedirect.com
ScienceDirect
Acta Materialia 55 (2007) 3111–3119
Acta MATERIALIA
www.elsevier.com/locate/actamat

Mathematical modeling of liquid phase migration in solid–liquid mixtures: Application to the sintering of functionally graded WC–Co composites

Peng Fan, Zhigang Zak Fang *, H.Y. Sohn

Department of Metallurgical Engineering, University of Utah, Salt Lake City, UT 84112, USA

Received 3 October 2006; received in revised form 28 December 2006; accepted 4 January 2007
Available online 6 March 2007

Abstract

Liquid phase migration (LPM) is an interfacial-energy-driven flow that takes place in a solid–liquid two-phase system. This phenomenon is similar to but different from the well-known capillary-driven flow. Understanding and controlling LPM is crucial for liquid phase sintering of various functionally graded materials, including WC–Co, with composition gradients. To date, there have been few studies that focus on the LPM phenomenon, partially because it is a complex process that involves mass transport with moving boundaries and changing volumes. This paper describes a quantitative study on the kinetics of LPM. The governing equation for LPM that takes into account the changes in volume was derived and a novel ''grid-tracking'' numerical technique was also developed for solving the governing equation. The methodology and techniques described in this paper can be applied to simulate and predict the kinetics of LPM during liquid phase sintering and the composition gradients as the result of LPM.

Keywords: Liquid phase migration; Liquid phase sintering; Functionally graded materials; Composites

1. Introduction

Liquid phase migration (LPM) is a physical phenomenon that takes place in a solid–liquid two-phase system consisting of an aggregate of solid grains filled with a liquid phase. In such a system the liquid phase tends to flow from a region with a higher liquid volume fraction and/or larger solid grains to a region with a lower liquid volume fraction and/or smaller solid grains. LPM is similar to but different from the well-known capillary-driven flow in porous media, because LPM can occur in solid–liquid two-phase systems in the absence of any pore space, while the classic capillary-driven flow results from the interaction among three phases: solid, liquid and gas.

LPM was first observed during the study of the manufacture of functionally graded cemented tungsten carbide [1–5] using a liquid phase sintering process with the objective of obtaining a composition gradient. It has also been known in the industry [3–5] that the liquid cobalt phase flows from a region with higher cobalt content or finer grain sizes to a region with lower cobalt content or coarser grain sizes during the liquid phase sintering of WC–Co. Fundamental understanding of the principles behind the LPM phenomenon, however, is lacking. This lack of knowledge in turn makes it difficult to control LPM during sintering or to make use of the phenomenon for the design of advanced materials. Therefore, understanding and controlling LPM is crucial for the manufacture of functionally graded WC–Co and other materials [6–10]. On the one hand, LPM can be exploited to create and control the composition gradient within a material; on the other hand, it can cause distortion and undesired inhomogeneity and defects within the material. To date, however, there are few studies that focus on the LPM phenomenon, partially because it is a complex process that involves mass transport with moving boundaries and changing volumes.

* Corresponding author. Tel.: +1 801 581 8128; fax: +1 801 581 4937.
E-mail address: zfang@mines.utah.edu (Z.Z. Fang).

1359-6454/$30.00
doi:10.1016/j.actamat.2007.01.015

Nomenclature

A	cross-sectional area (m^2)	V	volume (m^3)
d	grain size (m)	μ	viscosity ($kg\ m^{-1}\ s^{-1}$)
k_p	permeability (m^2)	v	velocity of liquid flow ($m\ s^{-1}$)
l	length (m)		
P_m	liquid migration pressure (Pa)	*Subscripts*	
t	time (s)	0	at time zero
u	liquid volume fraction ($=V_l/(V_l+V_s)$, where V_l and V_s are liquid volume and solid volume, respectively)	l	liquid
		s	solid

In this paper, we present a quantitative study on the kinetics of LPM. We will first describe the driving force for LPM. Then, the governing equation for LPM that takes into account the changes in volume is derived. A numerical solution method – the grid-tracking technique – for moving boundary conditions is developed. In the final section, we will present the simulation results on composition gradients in liquid phase sintering of WC–Co composite materials.

2. Driving force for LPM

When a porous medium is put in contact with a liquid pool, the liquid will be imbibed into the porous medium to fill in the pores, assuming the liquid wets the porous medium. This spontaneous imbibition of a liquid into a porous medium is attributed to the capillary force at the solid–liquid–gas interface and thus is termed the capillary-driven flow. Capillary-driven flow is important in many industries such as paper printing, textiles, filtration, contamination control and oil recovery [11–14]. Spontaneous liquid imbibition can also occur in a solid–liquid two-phase mixture without involving a gas phase. For example, it was shown that, when a fully densified, porosity-free mixture of solid WC grains in a liquid Co matrix at 1400 °C was put into contact with a Co melt pool at the same temperature, the composite body imbibed a large amount of liquid Co and expanded [3]. This type of spontaneous liquid imbibition is distinctly different from the conventional capillary-driven flow that involves interactions among three phases (i.e., two fluids and a solid). The term "liquid phase migration" (LPM) is used specifically to refer to the flow of the liquid phase in these situations, so as to distinguish it from that in a gas-filled porous medium [3].

The thermodynamic driving force for LPM in a solid–liquid two-phase system can be attributed to the reduction of the total interfacial energy of the system [3,15,16]. This driving force can be described using the term "liquid migration pressure" [3,4]. Fig. 1 schematically explains the driving force for this phenomenon, as demonstrated by the spontaneous liquid imbibition when a fully densified composite material is immersed in a melt whose composition is the same as the liquid phase inside the composite material. As shown in Fig. 1a, before LPM occurs the small liquid volume inside the composite material causes a high solid–solid interfacial area and a small solid–liquid interfacial area and, consequently, a high total interfacial energy of the system. Thus, the liquid migration pressure inside the composite material, $(P_m)_{in}$, is higher than the liquid migration pressure outside, $(P_m)_{out}$. This difference in liquid migration pressures will drive the liquid to flow into the composite material from outside. Accompanying the

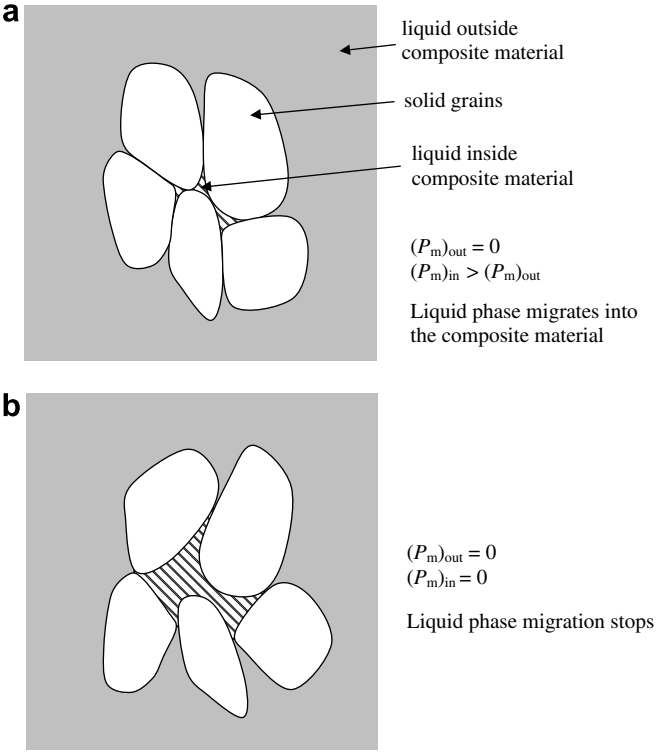

Fig. 1. Schematic drawing explaining the driving force for the LPM phenomenon, as demonstrated by the spontaneous imbibition of liquid when a fully densified sintered composite material is immersed in a melt whose composition is the same as the liquid phase inside the composite material. (a) Before LPM occurs. (b) After LPM stops.

liquid imbibition and the consequent increases in both liquid volume and total volume of the composite material, as shown in Fig. 1b, the solid grains are re-oriented to decrease the solid–solid interfacial area and increase the solid–liquid interfacial area. Consequently, this process decreases both the total interfacial energy and $(P_m)_{in}$. If there is sufficient liquid, liquid imbibition will not stop until the total interfacial energy reaches the minimum value when the solid–solid interfacial area vanishes completely. At that time, $(P_m)_{in}$ becomes zero and equal to $(P_m)_{out}$, thus eliminating the difference in liquid migration pressures inside and outside the composite material. Therefore, the driving force for LPM can be attributed to a reduction in the total interfacial energy of the system or a difference in liquid migration pressures of different regions in the system. The statement that the total interfacial energy decreases with increasing solid–liquid interface area and decreasing solid–solid interface area is based on the assumption that the liquid wets the solid grains. This assumption holds true for most composite materials.

The higher the liquid migration pressure, the stronger the imbibing force the system exerts on the external liquid. In other words, the liquid migration pressure may also be called the imbibition pressure. The liquid migration pressure of a liquid without solid grains is zero and the liquid migration pressure of a composite material with a very high volume fraction of the liquid phase such that the contact between solid grains completely vanishes is also zero. If the liquid migration pressure is not uniform within a system, liquid will flow from a region with a lower liquid migration pressure to a region with a higher liquid migration pressure, until the liquid migration pressure becomes uniform everywhere in the system.

3. Governing equation and numerical solution method

3.1. Governing equation

In order to describe the LPM phenomenon quantitatively, the governing equation that describes it has to be established. The challenge for establishing the governing equation of LPM lies in the fact that LPM is always accompanied by changes in shape and volume of the system, as illustrated in Fig. 2. The volume and shape changes will result in changes in the length in the direction of the LPM and the area across which the liquid phase migrates, which in turn lead to a considerably greater complexity when attempting to establish and solve the governing equation. Mathematically, this problem belongs to a category of moving boundary problems with variable volumes and shapes [17].

The solid–liquid system can be viewed as consisting of two parts: one is the solid phase skeleton consisting of all solid grains; the other is the liquid phase filling in the skeleton. To model LPM in such a system, three assumptions are made: first, that the solid phase skeleton is not rigid, in other words the grains that make up the skeleton are not rigidly bound together, but separable during the process; second, that the grain shapes and sizes are held constant; and, third, that there is no chemical gradient within the system except that the volume fraction of the liquid phase may vary with locations. These assumptions are reasonable with respect to real-life materials. Further validation of these assumptions will be given in Section 5.

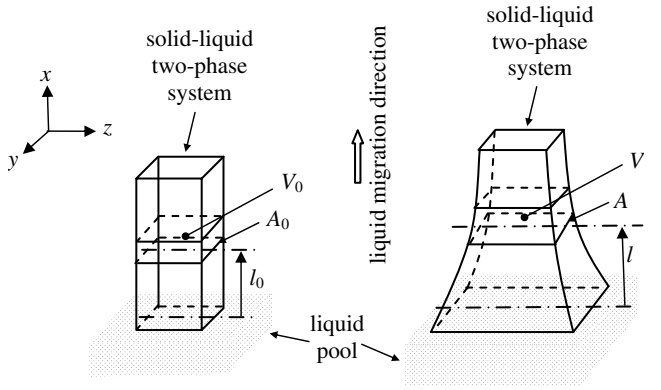

Fig. 2. Schematic of changes in shape and volume of a solid–liquid two-phase system during LPM. Here, the bottom side of the system is put in contact with a liquid pool. The system imbibes the liquid, its volume expands and thus the shape changes. At time zero, the distance of an arbitrarily selected control volume with a volume of V_0 and a cross-sectional area of A_0 is l_0 from the bottom. After LPM, the volume, the cross-sectional area and the distance become V, A and l, respectively.

Because the solid phase skeleton is not rigid, the skeleton can expand or shrink depending on the volume of liquid phase enclosed within it. This means that, relative to any fixed space coordinate, the solid phase skeleton has a velocity that varies with time and location and is dependent on the rate of the liquid phase flow; and the absolute velocity of liquid phase flow is the combination of its velocity relative to the skeleton and the velocity of the skeleton relative to the fixed coordinate. The coupling between the velocities of the skeleton and the liquid phase makes it difficult to establish the governing equation for LPM using fixed space coordinates.

To overcome this hurdle, we use a moving coordinate l in the direction of LPM (see Fig. 2). In this coordinate, the motion at any point is relative to the solid phase skeleton at that point and thus the velocity of the solid phase skeleton at any point is zero. By doing this, the space coordinate is attached to the solid phase skeleton and thus the velocity of the liquid phase is relative to the skeleton. Therefore, for any arbitrarily selected control volume in this coordinate, the volume of the solid phase skeleton is constant because of its zero velocity. Consequently, the volume change of the selected control volume results solely from imbibing the liquid, bridging the relations between the volume, the cross-sectional area and the liquid volume fraction in the control volume.

We assume one-dimensional liquid migration in the x-direction. By defining the lengths of the sides of a control volume (in Fig. 3), as Δl, Δl_y and Δl_z, respectively, the

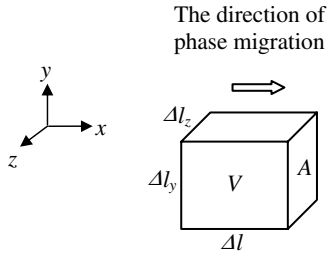

Fig. 3. Control volume.

volume, V, and the cross-sectional area perpendicular to the direction of LPM, A, are

$$V = \Delta l \Delta l_y \Delta l_z \tag{1}$$

$$A = \Delta l_y \Delta l_z \tag{2}$$

Based on conservation of the liquid volume, V_l, in the control volume, we obtain

$$\frac{dV_l}{dt} + \Delta l \frac{\partial}{\partial l}(vA) = 0 \tag{3}$$

where v is the velocity of the liquid flow relative to the skeleton consisting of solid grains.

Since the solid volume, V_s, in the control volume remains constant, we get

$$\frac{dV}{dt} = \frac{d}{dt}(V_l + V_s) = \frac{dV_l}{dt} \tag{4}$$

Therefore, Eq. (3) can be rewritten as

$$\frac{dV}{dt} + \Delta l \frac{\partial}{\partial l}(vA) = 0 \tag{5}$$

Assuming that volume expansion or shrinkage is uniform in the x-, y- and z-directions, we get

$$\Delta l_y = c_1 \Delta l \tag{6}$$

$$\Delta l_z = c_2 \Delta l \tag{7}$$

where c_1 and c_2 are constants which are independent of time.

Introducing Eqs. (6) and (7) into Eqs. (1) and (2) leads to

$$V = \Delta l \Delta l_y \Delta l_z = c_1 c_2 \Delta l^3 \tag{8}$$

$$A = \Delta l_y \Delta l_z = c_1 c_2 \Delta l^2 \tag{9}$$

Thus,

$$\frac{dV}{dt} = \frac{d}{dt}(c_1 c_2 \Delta l^3) = 3\Delta l^2 c_1 c_2 \frac{d(\Delta l)}{dt} \tag{10}$$

$$\frac{dA}{dt} = \frac{d}{dt}(c_1 c_2 \Delta l^2) = 2\Delta l c_1 c_2 \frac{d(\Delta l)}{dt} \tag{11}$$

Comparing Eqs. (10) and (11) leads to

$$\frac{dV}{dt} = \frac{3}{2}\Delta l \frac{dA}{dt} \tag{12}$$

Introducing Eq. (12) into Eq. (5) and re-arranging, we get

$$\frac{\partial A}{\partial t} = -\frac{2}{3}\frac{\partial}{\partial l}(vA) \tag{13}$$

Assuming that Darcy's law on liquid flow in porous media is applicable to this system, the velocity of the liquid flow relative to the skeleton consisting of solid grains, v, should be proportional to the gradient of the liquid migration pressure, P_m, with respect to l, that is,

$$v = \frac{k_p}{\mu}\frac{\partial P_m}{\partial l} \tag{14}$$

where k_p is permeability and μ is the viscosity of liquid.

Replacing v in Eq. (13) with

$$\frac{k_p}{\mu}\frac{\partial P_m}{\partial l}$$

according to Eq. (14) leads to

$$\frac{\partial A}{\partial t} = -\frac{2}{3}\frac{\partial}{\partial l}\left[A\frac{k_p}{\mu}\frac{\partial P_m}{\partial l}\right] \tag{15}$$

which can be rewritten as

$$\frac{\partial A}{\partial t} = -\frac{2}{3}\left[\frac{\partial}{\partial l}\left(\frac{k_p A}{\mu}\right)\frac{\partial P_m}{\partial l} + \frac{k_p A}{\mu}\frac{\partial^2 P_m}{\partial l^2}\right] \tag{16}$$

In Eq. (16), A, P_m and k_p are all dependent on liquid volume fraction, $u = V_l/(V_l + V_s)$.

The relation between the cross-sectional area, A, and the liquid volume fraction, u, is derived by the following procedure. The volume of solid phase, V_s, in the control volume, V, remains constant. Therefore,

$$V_s = V(1-u) = V_0(1-u_0) \tag{17}$$

Thus,

$$\frac{V}{V_0} = \frac{1-u_0}{1-u} \tag{18}$$

Based on Eqs. (8) and (9), we get

$$\frac{V_0}{V} = \left(\frac{\Delta l_0}{\Delta l}\right)^3 \tag{19}$$

$$\frac{A_0}{A} = \left(\frac{\Delta l_0}{\Delta l}\right)^2 \tag{20}$$

where the subscript 0 indicates time zero.

Comparing Eqs. (19) and (20) leads to

$$\frac{V_0}{V} = \left(\frac{A_0}{A}\right)^{1.5} \tag{21}$$

Introducing Eq. (21) into Eq. (18) and re-arranging, the relation between A and u is obtained to be

$$A = A_0\left(\frac{1-u_0}{1-u}\right)^{2/3} \tag{22}$$

where A_0 and u_0 are, respectively, the cross-sectional area and the liquid volume fraction at time zero.

Finally, introducing Eq. (22) into Eq. (16) and re-arranging, the following equation is obtained:

$$A_0(1-u_0)^{2/3}\frac{\partial(1-u)^{-2/3}}{\partial t}=-\frac{2}{3}\left[\frac{\partial}{\partial l}\left(\frac{k_p}{\mu}\left(\frac{1-u_0}{1-u}\right)^{2/3}A_0\right)\frac{\partial P_m}{\partial l}+\frac{k_p}{\mu}\left(\frac{1-u_0}{1-u}\right)^{2/3}A_0\frac{\partial^2 P_m}{\partial l^2}\right] \quad (23)$$

where A_0 is cross-sectional area perpendicular to the LPM direction at initial time (m^2); t is time (s); u is liquid volume fraction ($=V_l/(V_l+V_s)$, where V_l and V_s are liquid volume and solid volume, respectively); u_0 is liquid volume fraction at initial time; l is the distance in the LPM direction (m); k_p is the permeability of the system, in units of m^2; μ is the viscosity of liquid (kg m^{-1} s^{-1}); and P_m is the liquid migration pressure (Pa). Since P_m and k_p are both dependent on liquid volume fraction u, Eq. (23) is an equation with u as the dependent variable and t and l as the independent variables.

This equation is the governing equation of LPM that is applicable to any material system that satisfies the three basic assumptions. It is noted, however, that the governing equation has been derived without any assumptions with regard to microstructure parameters such as dihedral angles and the shapes of the grains. The effect of the microstructure parameters of the material system is implicit by their effects on the values of P_m and k_p.

3.2. Numerical solution method

The governing equation of LPM, i.e., Eq. (23), is a nonlinear partial differential equation and thus can only be solved numerically. The finite-difference method, more specifically the MacCormack method – an explicit two-step (i.e., predictor–corrector) method that has been proved very efficient and thus popular for solving nonlinear partial differential equations [18] – was used in this study. It should be noted that l, the distance from one end of the two-phase system, varies with time, as shown in Fig. 2. Its value must be obtained by summing up the values of Δl which are updated for each time-step according to the following relation, obtained by introducing Eq. (20) into Eq. (22):

$$\Delta l=\Delta l_0\left(\frac{1-u_0}{1-u}\right)^{1/3} \quad (24)$$

Since the space coordinates of all grid points are tracked (i.e., updated) for each time-step, this method can be termed the "grid-tracking technique". The finite-difference equation of the governing equation of LPM, i.e., Eq. (23), and the detailed solution algorithm is given in Appendix A.

4. Simulation results

Eq. (23) is a general governing equation for LPM, indicating that it can be applied to describe the LPM phenomenon occurring in any solid–liquid two-phase systems. The numerical solution of this equation is, of course, dependent on the characteristics of specific system, since both liquid migration pressure, P_m, and permeability, k_p, are dependent on specific physical parameters of the system. In this study, the cemented tungsten carbide system (WC–Co) was used as the model system because of its wide-ranging industrial applications [19,20].

The dependence of liquid migration pressure on the solid grain size and the liquid volume fraction in the WC–Co system is obtained as follows [21]:

$$P_m=2048\lfloor(1/u-1)^{1/3}-1.41u\rfloor/d^{0.4} \quad (25)$$

where P_m is in Pa and d is in m. This equation and the values of the constants in the equation are determined experimentally for the WC–Co system. They depend implicitly on the properties of the materials and the geometric shape of the grains.

According to Rumpf and Gupte [22], the relation between the permeability, k_p, the liquid volume fraction, u, and the solid grain diameter, d, can be expressed as

$$k_p=cd^2u^m \quad (26)$$

where c and m are constants. Note that Eq. (26) is a semi-empirical relation which has been applied extensively to a large variety of porous media including loosely packed particles, filters, rocks and so on. The values of c and m are typically determined on a case-by-case basis for each specific different material system [12,23,24]. During liquid phase sintering at high temperatures, cemented tungsten carbide – the model material of the present study – consists of a solid WC skeleton and liquid cobalt, which occupies interstitial places between WC grains. It is assumed that the WC skeleton is not rigid. Therefore, the WC–Co system is similar to many systems of loosely packed particles to which the Rump and Gupte equation has been successfully applied. The Rump and Gupte equation is hence applied to study the liquid flow in the WC–Co system during sintering. The values of c and m for WC–Co can be determined through the following best-fitting procedure based on reported data of the liquid migration rate experiments on WC–Co [3]. For any sets of values of c and m, the corresponding solutions can be obtained by substituting Eqs. (25) and (26) into the governing equation for the LPM – i.e., Eq. (23) – and solving it using the numerical technique described in Section 3.2. Comparison of the numerical solution and the reported experimental data on liquid migration [3] leads to the best-fit values of c and m as $c=4.5\times10^{-4}$ and $m=1.5$. Thus, the permeability for the WC–Co system can be expressed as

$$k_p=4.5\times10^{-4}d^2u^{1.5} \quad (27)$$

where d is WC grain size (m) and k_p is permeability (m^2). Now we can predict the formation and/or elimination of the Co gradient during the liquid phase sintering of WC–Co.

A set of experimental results were reported by Lisovsky [3] for fully densified WC–Co sintered bars imbibing Co melt after one side of the WC–Co bar was put into contact

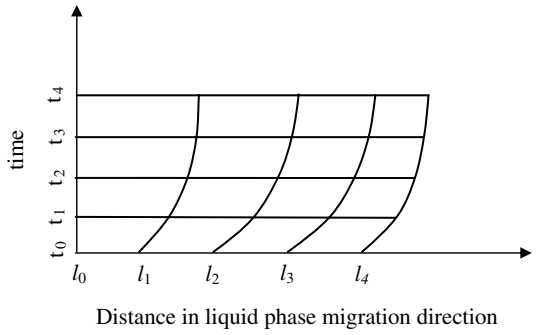

Fig. 4. Finite-difference grid used in the numerical solution of the governing equation, with a fixed and equal time-step, but variable and unequal spatial steps.

with the Co melt; l is the distance from the contacting interface between the WC–Co bar and the Co melt; u is the liquid Co volume fraction in the WC–Co bar. The initial Co content in the WC–Co was 5.9 wt% and the saturated Co content in WC–Co was 32 wt%. The volume fraction of liquid Co was calculated from the molar volumes and mole fractions of WC and liquid Co. The molar volume of liquid Co depends on its composition, which was determined from W–Co–C ternary phase diagram [25]. The molar volumes of the pure elemental Co, C and W in the liquid Co phase (which are also needed for the calculation of the molar volume of liquid Co) and the molar volume of WC are all available in the literature [26]. The viscosity of liquid Co is also available in the literature [27]. Fig. 5 shows that the model prediction agrees well with the experimental results on liquid imbibition into fully densified sintered materials.

Another simulation was conducted for an 8 mm thick WC–Co bi-layer specimen. The specimen had a built-in Co gradient in the green part. The grain size of WC was the same in both layers (with average WC grain size – linear intercept length – of 2 μm after liquid phase sintering for 5 min). The results of the simulation as illustrated by Fig. 6 show that the cobalt gradient changes with the time of sintering. Initially, Co contents in the two layers were 6% and 16%, respectively. As the sintering time increased, the Co gradient decreased. The Co gradient was eliminated completely in 6 min. This result is again consistent with our experimental results, which showed that the cobalt gradient was eliminated in 5 min.

The good agreement between the simulated and experimental results mentioned above validates the use of the model to predict the variation of Co gradient in WC–Co materials as functions of the grain size, initial Co content distribution, the sample thickness and length of sintering period. Fig. 7 illustrates the prediction of transient Co gradients for two 20 mm thick WC–Co bi-layers, one (Fig. 7a) with identical WC grain sizes but different initial Co contents and the other (Fig. 7b) with identical initial Co contents but different WC grain sizes.

5. Discussion

As mentioned earlier, the above derivation and solution of the LPM problem was based on three basic assumptions. The validity of these three assumptions, hence the relevance of the present work to real-life materials, is further discussed as follows.

First, the solid phase skeleton consisting of all solid grains is flexible rather than rigid. In other words, the grains that make up the skeleton are separable during the LPM process such that the skeleton can expand or shrink depending on the volume of liquid phase enclosed in the skeleton. This assumption is undoubtedly true at relatively low temperatures for solid–liquid two-phase systems because there are no rigid bondings between the grains. During liquid phase sintering at higher tem-

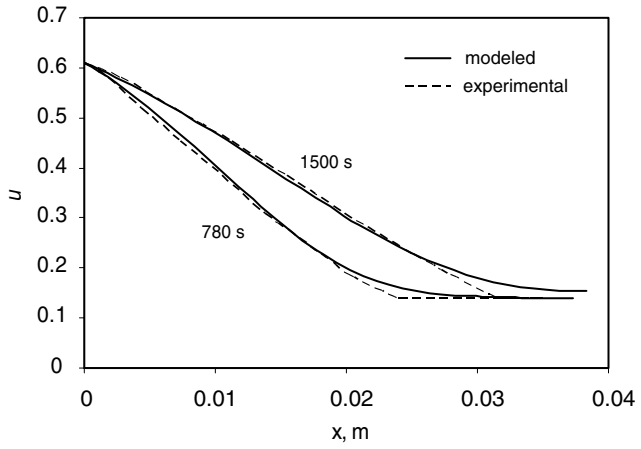

Fig. 5. Comparison between the simulation in this study and the experimental results of Lisovsky [3] on the rate of LPM in the WC–Co system.

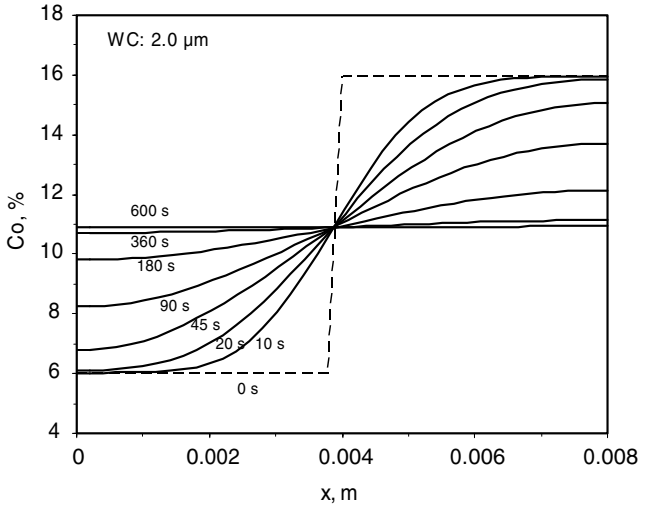

Fig. 6. Predicted distribution of Co content profile in an 8 mm thick WC–Co bilayer with identical WC grain sizes, but different initial Co contents sintered at 1400 °C for different time periods.

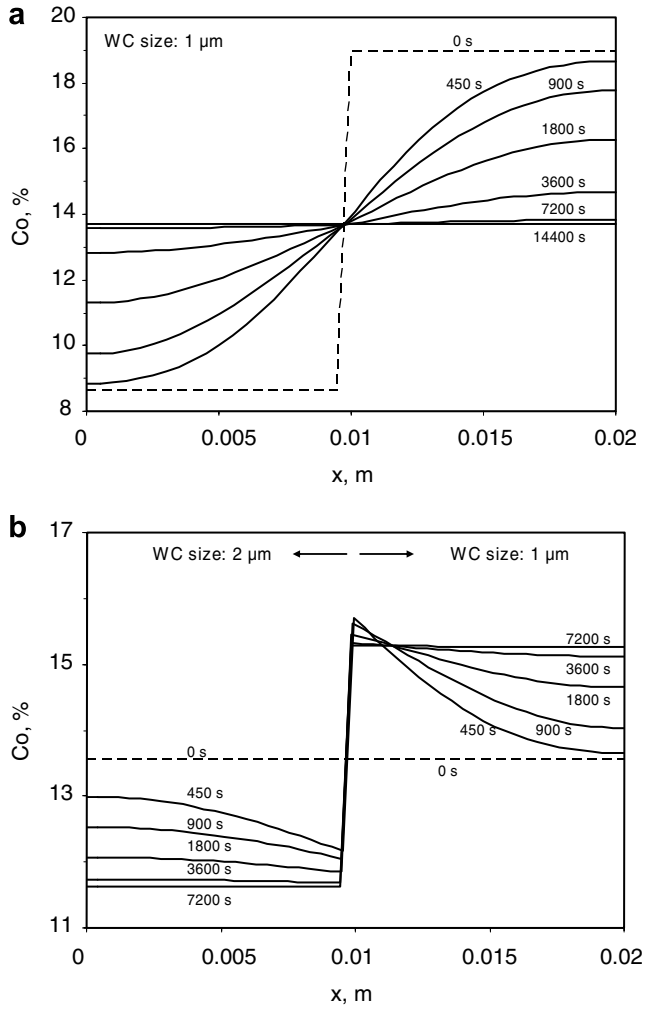

Fig. 7. Predicted distribution of Co content profiles in a 20 mm thick WC–Co bilayer sintered at 1400 °C for different time periods. (a) With identical WC grain sizes, but different initial Co contents; (b) with identical initial Co contents, but different WC grain sizes.

peratures, however, the contact between solid grains depends strongly on the dihedral angle between the solid phase and the liquid phase. For materials systems with the dihedral angle larger than zero, rigid bondings may form between grains after a period of sintering. For these systems, LPM can only occur before rigid intergranular bondings form, because a flexible skeleton consisting of separable grains is a prerequisite for LPM to be able to occur. When the dihedral angle is zero, however, as for materials systems such as many metal–ceramic and ceramic–ceramic composite materials such as WC–Co [3] and $SrTiO_3$–Nb_2O_5 [28], the liquid phase will penetrate the grain boundaries and form liquid films at the grain boundaries, so that all the grains are separated without forming rigid bonds between them [8,28]. The flexibility of the solid phase skeleton has also been experimentally demonstrated by Lisovsky's experiment of dipping a fully densified WC–Co specimen in a liquid pool of cobalt and showing that the sintered body swells because of the imbibition of the liquid Co [3]. In short, the present model can be applied to many materials systems depending on the value of the dihedral angle of the system.

In Section 2, it was mentioned that LPM is driven by the reduction of total interfacial energy of the system, through decreasing solid–solid interface area and increasing solid–liquid interface area. However, when the dihedral angle is zero in materials such as WC–Co, the grain-to-grain contact consists of a liquid film [28]. The so-called solid–solid interface, in this case, should be more precisely termed a "solid-to-liquid-film interface". The interfacial energy of solid-to-liquid-film interface is different from that of the solid-to-bulk-liquid interface, since the properties and microstructure of liquid films are different from those of bulk liquid phase [28]. Therefore, the LPM can be attributed to the reduction of total interfacial energy of the system, through decreasing solid-to-liquid-film interface area and increasing solid-to-bulk-liquid interface area.

The second assumption of the present model is that the grain shape and size are held constant during the LPM process. For many materials systems, including WC–Co, this is reasonable because compared to the rate of liquid migration, the rate of grain growth is very slow [3,29]. In other words, the effect of the changes of grain shape and size lags behind the changes due to liquid migration. Liquid migration will be complete before grain shape and size will have changed significantly. For example, no significant changes in WC grain shape and size were observed in a WC–Co system that had undergone a considerable LPM [3]. Of course, for different materials systems this could be different. In a case where the sintering time is long or the change in grain shape and size is fast for any specific material system, the change of grain shape and size can be readily incorporated into the model if the rate of grain shape and size change as a function of time and other material parameters is available.

The third assumption is that the chemical compositions of the liquid phase and the solid grains are homogeneous throughout the composite. In other words, the LPM discussed in this paper is solely due to the differences in grain sizes and the nonuniformity of the distribution of the liquid phase within the composite. In practice, this type of LPM, involving no chemical gradients or chemical changes, is well-known in industry [5,6], although not well understood. It is important to note, however, that LPM may also be induced if there were chemical gradients within the material in the absence of any differences in grain size or volume fraction of the liquid phase. For example, migration of liquid Co will occur in TiN containing WC–Co materials during liquid phase sintering in which the Co migration is attributed to Co and Ti diffusion associated with the chemical gradient of titanium and nitrogen [30–34]. This type of LPM induced by chemical gradients is beyond the scope of this paper.

6. Summary

A mathematical model that describes the rate of LPM has been formulated. A governing equation that takes into account the changes in volume has been derived and a novel "grid-tracking" numerical technique has been developed for solving the governing equation. The model successfully describes the LPM in a solid–liquid phase mixture as a function of grain size and liquid volume fraction. The dependence of the LPM process on the grain size and volume fractions and the compositional gradients in a liquid-phase-sintered composite as a result of LPM can be numerically simulated and this simulation can in turn be used for the design and manufacture of functionally graded materials. The results of the simulations of the transient composition gradients during liquid phase sintering of WC–Co agree well with the reported experimental data. The method described in this paper can also be applied to the modeling of other composite materials, if the dependences of the liquid migration pressure and the permeability on grain size and liquid volume fraction are known by either experimental measurement or theoretical estimation.

Acknowledgements

The authors wish to thank the US Department of Energy, Industrial Materials of the Future Program, for its financial support. We also acknowledge the contributions of Kennametal Inc. and Smith International Inc. for providing in-kind financial support.

Appendix A. Numerical solution method of the governing equation of LPM

In this study, the governing equation of LPM, i.e., Eq. (23), was solved numerically by a finite-difference method, the MacCormack method – an explicit two-step (i.e., predictor–corrector) method that has been proved very efficient and thus popular for solving nonlinear partial differential equations [18].

The finite-difference equations for the predictor and the corrector steps are obtained to be Eqs. (A1) and (A2), respectively, as follows:

$$(1-u_i^{\overline{n+1}})^{-2/3} = (1-u_i^n)^{-2/3} + \Delta t (A_0)_i^{-1}(1-(u_0)_i)^{-2/3}\left(-\frac{2}{3}\right)\frac{1}{\mu} \times \left\{ \left[\frac{(1-(u_0)_{i+1})^{2/3}(A_0)_{i+1}\frac{(k_p)_{i+1}^n}{(1-u_{i+1}^n)^{2/3}} - (1-(u_0)_i)^{2/3}(A_0)_i\frac{(k_p)_i^n}{(1-u_i^n)^{2/3}} }{ l_{i+1}^n - l_i^n } \right] \times \frac{(P_m)_{i+1}^n - (P_m)_i^n}{l_{i+1}^n - l_i^n} + \frac{(1-(u_0)_i)^{2/3}(A_0)_i}{(1-u_i^n)^{2/3}} \left[\frac{2(P_m)_{i-1}^n}{(l_{i-1}^n - l_i^n)(l_{i-1}^n - l_{i+1}^n)} + \frac{2(P_m)_i^n}{(l_i^n - l_{i-1}^n)(l_i^n - l_{i+1}^n)} + \frac{2(P_m)_{i+1}^n}{(l_{i+1}^n - l_{i-1}^n)(l_{i+1}^n - l_i^n)} \right] \right\} \quad \text{(A1)}$$

$$(1-u_i^{n+1})^{-2/3} = 0.5 \times \left\langle (1-u_i^n)^{-2/3} + (1-u_i^{\overline{n+1}})^{-2/3} + \Delta t (A_0)_i^{-1}(1-(u_0)_i)^{-2/3}\left(-\frac{2}{3}\right)\frac{1}{\mu} \times \left\{ \left[\frac{(1-(u_0)_i)^{2/3}(A_0)_i\frac{(k_p)_i^{\overline{n+1}}}{(1-u_i^{\overline{n+1}})^{2/3}} - (1-(u_0)_{i-1})^{2/3}(A_0)_{i-1}\frac{(k_p)_{i-1}^{\overline{n+1}}}{(1-u_{i-1}^{\overline{n+1}})^{2/3}} }{ l_i^{\overline{n=1}} - l_{i-1}^{\overline{n+1}} } \right] \frac{(P_m)_{i+1}^{\overline{n+1}} - (P_m)_i^{\overline{n+1}}}{l_i^{\overline{n+1}} - l_{i-1}^{\overline{n+1}}} + \frac{(1-(u_0)_i)^{2/3}(A_0)_i}{(1-u_i^{\overline{n+1}})^{2/3}} \left[\frac{2(P_m)_{i-1}^{\overline{n+1}}}{(l_{i-1}^{\overline{n+1}} - l_i^{\overline{n+1}})(l_{i-1}^{\overline{n+1}} - l_{i+1}^{\overline{n+1}})} + \frac{2(P_m)_i^{\overline{n+1}}}{(l_i^{\overline{n+1}} - l_{i-1}^{\overline{n+1}})(l_i^{\overline{n+1}} - l_{i+1}^{\overline{n+1}})} + \frac{2(P_m)_{i+1}^{\overline{n+1}}}{(l_{i+1}^{\overline{n+1}} - l_{i-1}^{\overline{n+1}})(l_{i+1}^{\overline{n+1}} - l_i^{\overline{n+1}})} \right] \right\} \right\rangle \quad \text{(A2)}$$

where the subscripts $i-1$, i and $i+1$ denote the space grid lines; the superscript n and $n+1$ denote the time grid lines; and the superscript $\overline{n+1}$ denotes provisional (i.e., predicted) values for the $n+1$ time grid line, calculated from Eq. (A1) at the predictor step. Due to the differences in expansion or shrinkage at each space point, the space grid is nonuniform – as shown in Fig. 4 – and thus the second-order space derivative in the partial differential equation (i.e., Eq. (23)) was approximated by Lagrange-type polynomials [18].

It should be noted that l, the distance from one end of the two-phase system, varies with time, as shown in Fig. 2. Its value must be obtained by summing up the values of Δl which are updated for each time-step according to the following relation, obtained by introducing Eq. (20) into Eq. (22):

$$\Delta l = \Delta l_0 \left(\frac{1-u_0}{1-u} \right)^{1/3} \quad (24)$$

Using the average values of u_i and u_{i-1} (i.e., $0.5(u_i + u_{i-1})$) to replace u values between grids i and $i-1$, Eq. (24) can be written as Eqs. (A3) and (A4), for the predictor and the corrector steps, respectively

$$l_i^{\overline{n+1}} - l_{i-1}^{\overline{n+1}} = [(l_0)_i - (l_0)_{i-1}] \left(\frac{1 - 0.5[(u_0)_i + (u_0)_{i-1}]}{1 - 0.5(u_i^{\overline{n+1}} + u_{i-1}^{\overline{n+1}})} \right)^{1/3} \quad \text{(A3)}$$

$$l_i^{n+1} - l_i^{n+1} = [(l_0)_i - (l_0)_{i-1}] \left(\frac{1 - 0.5[(u_0)_i + (u_0)_{i-1}]}{1 - 0.5(u_i^{n+1} + u_i^{n+1})} \right)^{1/3} \quad \text{(A4)}$$

Since the space coordinates of all grid points are tracked (i.e., updated) for each time-step, this method can be termed the grid-tracking technique.

The solution algorithm is listed below.

1. Input Δt, μ and d_i (solid grain size at each grid).
2. Input the initial values: $(u_0)i$, $(l_0)_i$ and $(A_0)_i$.
3. Start from time zero, i.e., $n = 1$. At this time, $u_i^n = (u_0)_i$ and $l_i^n = (l_0)_i$.
4. Calculate $(k_p)_i^n$ and $(P_m)_i^n$, based on the dependence of k_p and P_m on u and d (e.g., Eqs. (27) and (25) for the WC–Co system).
5. In the predictor step, firstly calculate $u_i^{\overline{n+1}}$ from Eq. (A1); then calculate $l_i^{\overline{n+1}}$ from Eq. (A3); and finally calculate $(k_p)_i^{n+1}$ and $(P_m)_i^{n+1}$.

6. In the corrector step, firstly calculate u_i^{n+1} from Eq. (A2); then calculate l_i^{n+1} from Eq. (A4); and finally calculate $(k_p)_i^{n+1}$ and $(P_m)_i^{n+1}$.
7. Let $t = t + \Delta t$, $u_i^n = u_i^{n+1}$, $l_i^n = l_i^{n+1}$, $(k_p)_i^n = (k_p)_i^{n+1}$ and $(P_m)_i^n = (P_m)_i^{n+1}$. Repeat steps (5)–(7), until required time t is reached.

Appendix B. Supplementary data

Supplementary data associated with this article can be found, in the online version, at doi:10.1016/j.actamat.2007.01.015.

References

[1] Lisovskii AF, Babich MM. Poroshkovaya Metallurgiya (Kiev) 1972;12:53.
[2] Lisovskii AF, Linenko YP. Poroshkovaya Metallurgiya (Kiev) 1972;12:38.
[3] Lisovsky AF. Powder Metall Int 1987;19:18.
[4] Lisovsky AF. Int J Heat Mass Transfer 1990;33:1599.
[5] Fang Z, Eso O. Scripta Mater 2005;52:785.
[6] Suresh S, Mortensen A. Fundamentals of functionally graded materials. London: IOM Communications; 1998.
[7] Suresh S. Science 2001;292:2447.
[8] German RM. Sintering theory and practice. New York: John Wiley & Sons; 1996.
[9] Lee JH, Lee JH, Jung YS, Kim DY. J Am Ceram Soc 2003;86:1518.
[10] Kim JJ, Harmer MP. J Am Ceram Soc 1998;81:205.
[11] Grathwohl P. Diffusion in natural porous media. Boston, MA: Kluwer Academic Pub; 1998.
[12] Dullien FAL. Porous media: fluid transport and pore structure. San Diego, CA: Academic Press; 1992.
[13] Stange M, Dreyer ME, Rath HJ. Phys Fluids 2003;15:2587.
[14] Alava M. Adv Phys 2004;53:83.
[15] Delannay F, Pardoen D, Colin C. Acta Mater 2005;53:1655.
[16] Park HH, Yoon DN. Metall Trans A 1985;16A:923.
[17] Crank J. Free and moving boundary problems. Oxford: Oxford University Press; 1984.
[18] Hoffman JD. Numerical methods for engineers and scientists. New York, NY: Marcel Dekker; 2001. p. 670.
[19] Cheng J, Wu Y, Xia Y. Mater Sci Forum 2003;45–48:423.
[20] Upadhyaya GS. Cemented tungsten carbides: production, properties, and testing. Westwood, NJ: Noyes Publications; 1998.
[21] Fan P, Eso O, Fang ZZ, Sohn HY. Int J Refract Metal Hard Mater 2007, in press.
[22] Rumpf H, Gupte AR. Chem Ing Tech 1971;43:367.
[23] Mahale AE. Phase diagrams for ceramists. Am Ceram Soc 1994;vol. X:277.
[24] Mavko G, Nur A. Geophysics 1997;62:1480.
[25] Trussell RR, Chang M. J Environ Eng 1999;125:998.
[26] Uhrenius B. Int J Refract Metal Hard Mater 1993–1994;12:121.
[27] Turkdogan ET. Physical chemistry of high temperature technology. New York, NY: Academic Press; 1980. p. 108.
[28] Kang SJL. Sintering: densification, grain growth and microstructure. Boston, MA: Elsevier, Butterworth-Heinemann; 2005.
[29] Exner HE, Fischmeister H. Arch Eisen 1966;37:417.
[30] Suzuki H, Hayashi K, Taniguchi Y. Trans Jpn Inst Met 1981;22:758.
[31] Schwazkopf M, Exner E, Fischmeister H. Mater Sci Eng A 1988;105/106:225.
[32] Gustafson P, Ostlund A. In: Bildstein H, Eck R, editors. Proceedings of the 13th international Plansee seminar, Metallwerk Plansee, reutte, vol. 2. 1993. p. 537.
[33] Ekroth M, Frykholm R, Lindholm M, Andren HO, Agren J. Acta Mater 2000;48:2177.
[34] Frykholm R, Ekroth M, Janson B, Agren J, Andren HO. Acta Mater 2003;51:1115.